SUPPORTING INFORMATION

Optical Properties of PbS Nanocrystal Quantum Dots at Ambient and Elevated Pressure

Kaifu Bian[a], Benjamin T. Richards[b], Hanqing Yang[a], William Bassett[c], Frank W. Wise[d], Zhongwu Wang[e] and Tobias Hanrath[a*]

[a]School of Chemical and Biomolecular Engineering, [b]Department of Material Science and Engineering, [c]Department of Earth and Atmospheric Sciences, [d]School of Applied and Engineering Physics, [e]Cornell High Energy Synchrotron Source (CHESS), Cornell University, Ithaca, NY, 14853 [*]Corresponding Author

1. Experimental Methods

a. Synthesis of colloidal PbS NQDs

PbS NQDs used in this study were prepared following the method reported by Hines and Scholes.[1] In a typical synthesis resulted in the large (6.7 nm) PbS NQDs, 0.45 g of lead oxide (PbO) was dissolved in 20 mL of oleic acid (OA) and then heated up to 150°C to form a lead oleate solution. Then the solution was held at 150°C for one hour under nitrogen flow to degas. The solution was then cooled down to the reaction temperature of 130°C. In a nitrogen glovebox, 210 μL of bis(trimethylsilyl)sulfide (TMS) was dissolved in 10 mL of 1-octadecene (ODE) and then injected rapidly into the hot lead oleate solution. The liquid turned dark immediately after injection, indicating the formation of PbS NQDs. The raw product was collected after reaction for 1 min and then washed twice by sequential precipitation with ethanol and redispersed in hexane. Finally the solvent was removed by nitrogen flow and the dry NQDs were stored inside the nitrogen glovebox.

b. NQD Size Measurements by Transmission Electron Microscopy.

PbS NQDs were dispersed in hexane and drop-cast on carbon coated copper grids for transmission electron microscopy (TEM) imaging using a FEI Tecnai T-12 microscope. The diameters of NQDs are measured by statistics on at least 200 NQDs in TEM images. Figure S1 shows representative TEM images and the corresponding diameter histograms of the three samples used in this work.

c. In-situ High-Pressure Absorbance and X-ray Scattering Measurements.

High pressure environment was achieved by a diamond anvil cell (DAC) consisting of two aligned diamond anvils. A very small amount of saturated toluene suspension of PbS NQD was loaded into a 150-μm diameter hole drilled on a pre-indented stainless-steel gasket and then encapsulated and pressurized by the diamond anvils. Multiple ruby chips were placed in the gasket in the DAC with the sample to measure pressure using a well-known standard pressure dependent ruby fluorescence method. The pressure gradient within the sample chamber never exceeded 0.2 GPa in all measurements that involved in quantitative analysis.

Optical absorbance measurements were performed using a Varian Cary 5000 UV-vis-NIR spectrometer. A typical optical spectrum of PbS NQDs is shown in Figure 1b. The fine oscillation is due to light interference by the diamond culets. High-pressure X-ray scattering measurements were performed at the B1 beamline at Cornell High Energy Synchrotron Source (CHESS). A monochromatic X-ray of wavelength of 0.4859 Å was generated by two Ge (111) single crystals. Then the beam size was reduced to 100 μm by a collimator. Both small angle and wide angle X-ray scattering patterns from the samples were simultaneously collected by a large-area Mar345 image plate detector (Figure 1c). The sample-to-detector distance was calibrated using a CeO_2 standard to 779.2 mm. The scattering patterns were then integrated by Fit2D software[2] and analyzed.

2. Transmission Electron Microscopy Analysis of PbS NQDs

Representative TEM images and corresponding diameter histograms of the three samples used in this study are shown in Figure S1. The sizes of small, medium and large PbS NQDs are determined to be 3.0±0.3, 3.7±0.3 and 6.7±0.6 nm in diameter.

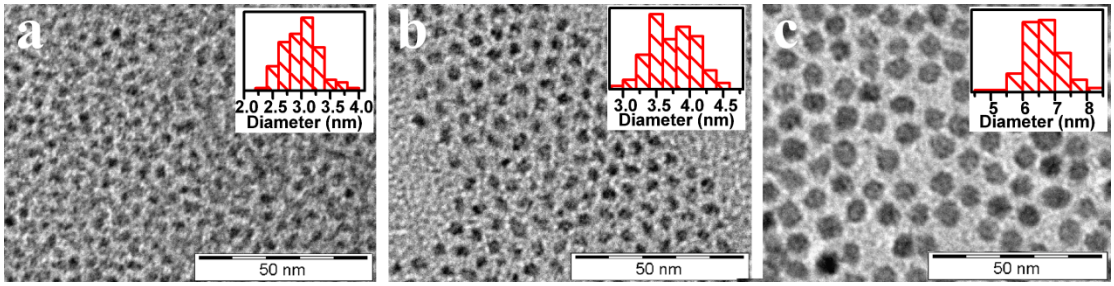

Figure S1. TEM images of (a) small, (b) medium and (c) large PbS NQDs. Insets shows histogram of NQD diameter by counting at least 200 NQDs.

3. Pressure-coefficient of the excitonic peak in the rock-salt phase

In the pressure range spanning from ambient to ~5 GPa, the pressure coefficients, $\left(\frac{\partial E_g}{\partial P}\right)_T$, were determined from linear fits to be -40.6, -50.1 and -61.0 meV/GPa, for small, medium and large NQDs, respectively (Figure S2).

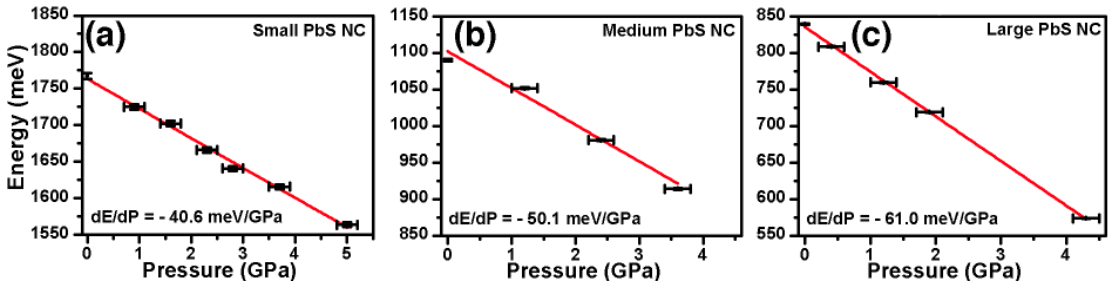

Figure S2. Fitted excitonic peak positions of absorption spectra shown in Figure 2 of the main text. Linear fits are indicated by red lines and the values of $\left(\frac{\partial E_g}{\partial P}\right)_T$ are shown in the figure.

4. *in-situ* High-Pressure Small-Angle X-ray Scattering

Figure S3 shows *in-situ* high-pressure SAXS spectra of small, medium and large PbS NQDs. The position of the first, and also the strongest, peak was determined by fitting for each spectrum and then used to calculate center-to-center distance d_{NN} between nearest neighbor NQDs under elevated pressures as shown in Figure 4a in the main text.

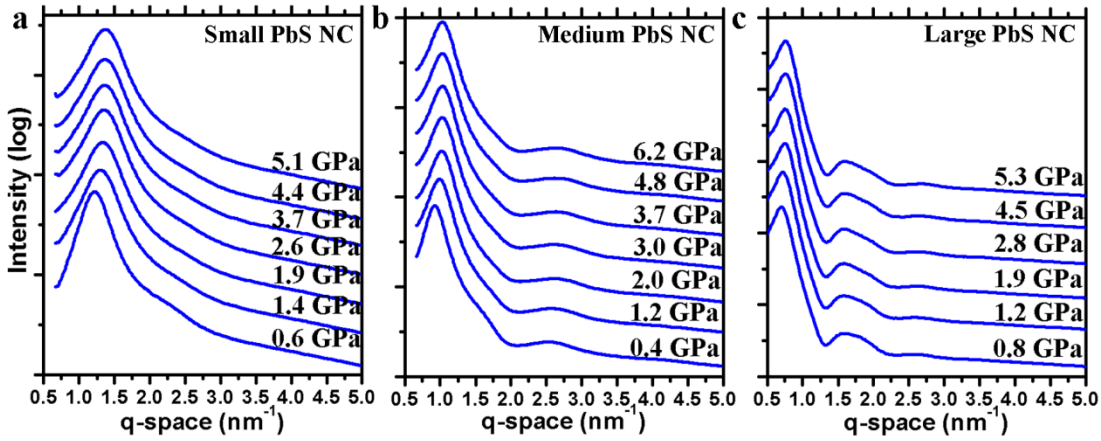

Figure S3. *in-situ* high-pressure SAXS spectra of (a) small, (b) medium and (c) large PbS NQDs.

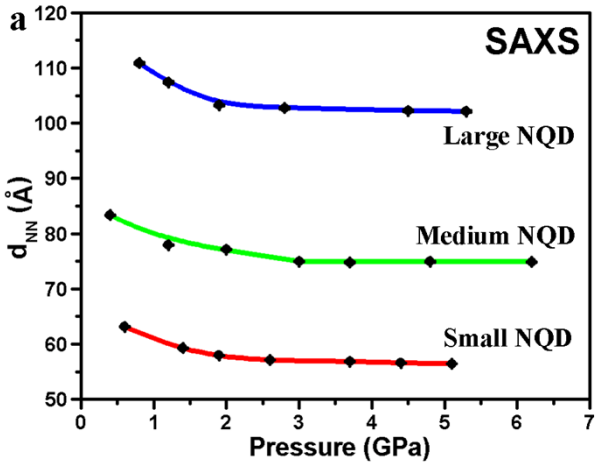

Figure S4. Center-to-center distance d_{NN} between nearest neighbor NQDs measured by *in-situ* high-pressure SAXS of small, medium and large PbS NQDs.

5. Comparing the basic model of the pressure coefficient to experimental data.

The basic model discussed in the main text approximates the pressure coefficient of the NQD exciton energy based on the bulk PbS parameters for pressure coefficient, bulk modulus and effective mass. Figure S5 shows that the basic model significantly overestimates the size-dependence of the pressure coefficient. The detailed model accounting for the size-dependent bulk modulus is detailed below.

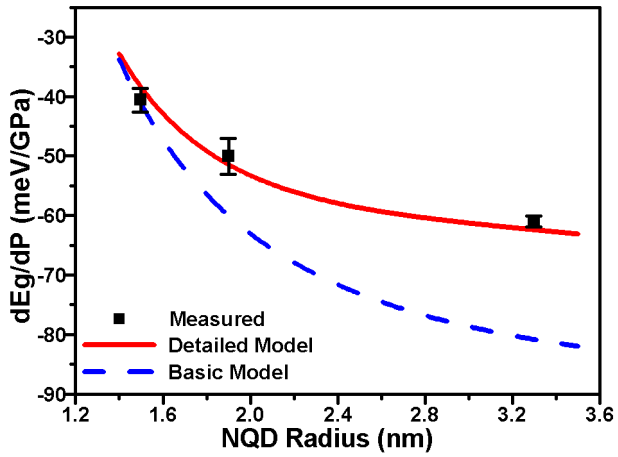

Figure S5. Experimental and theoretical values of size-dependent pressure variation of the energy gap of PbS NQDs. The blue dashed line shows the basic model (eqn. 2) with literature values for pressure coefficient and bulk modulus. The red line represents detailed model (eqn. S15, *vide infra*). The points calculated by the detailed model were fitted to a spline for visual aid.

6. Bulk moduli of PbS NQDs from WAXS results

To calculate bulk moduli of the PbS NQDs, the four peaks ({111}, {200}, {220} and {311} of the PbS rock salt lattice in each WAXS spectrum were fitted. The peak positions were then used to obtain the lattice constant by the software UnitCell.[3] Then the volume of a unit cell is calculated and normalized with respect to the ambient pressure value: $v(P) = V(P)/V_0 = [a(P)/a_0]^3$. $v(P)$ was then fitted to the Vinet equation of state (eqn. S1)[4,5] to determine bulk modulus B_0:

$$P = 3B_0 v^{-2/3}\left[1 - v^{1/3}\right]\exp\left\{1.5\left(B_0' - 1\right)\left[1 - v^{1/3}\right]\right\} \qquad \text{(S1)}$$

,where $B_0 = B|_{P=0}$ is the bulk modulus under ambient pressure, and $B'_0 = dB/dP|_{P=0}$ is the pressure derivative of the bulk modulus. In this study, B'_0 is fixed at 4.0 for fair comparison between samples.[6,7] The variable bulk modulus indicates size-dependence of mechanical properties of PbS NQDs which contribute to the size-dependence of the pressure coefficient dE_g/dP, as detailed in the main text.

7. Modeling $\left(\frac{\partial E_g}{\partial P}\right)_T$ of PbS NQDs

The energy gap of semiconductor NQDs can be approximated by the model introduced by Brus:[8]

$$E_g^{NQD} = E_g + \frac{\hbar^2\pi^2}{2\mu R^2} - \frac{1.8e^2}{\varepsilon_2 R} \qquad \text{(S2)}$$

Where $E_{g,NQD}$ is the intrinsic energy gap of the bulk semiconductor. The second term E_{con} presents the quantum confinement energy as a function of NQD radius R and reduced effective mass of electron-hole pair, μ of the semiconductor. For PbS $\mu = 0.0387m_0$ is the reduced mass, where m_0 is free electron mass[9]. The third term E_{ex} presents the Coulomb attraction between the electron and the hole, $\varepsilon_2 = 4\pi\varepsilon_{PbS}\varepsilon_0$ is the dielectric constant of PbS NQD. $\varepsilon_{PbS} = 17.9$ is the relative permittivity of PbS.

The pressure coefficient $dE_{g,NQD}/dP$ takes the form

$$\left(\frac{\partial E_{g,NQD}}{\partial P}\right)_T = \left(\frac{\partial E_g}{\partial P}\right)_T + \left(\frac{\partial E_{con}}{\partial P}\right)_T + \left(\frac{\partial E_{ex}}{\partial P}\right)_T \qquad \text{(S3)}$$

Figure S2 shows that $E_{g,QD}$ is linear to pressure within the pressure range of this work. Consequently $dE_{g,NQD}/dP$ is treated as constant and only the ambient pressure values need to be calculated, *i.e.*

$$\left(\frac{\partial E_{g,NQD}}{\partial P}\right)_T = \left.\frac{\partial E_{g,NQD}}{\partial P}\right|_{P=0} = \left.\frac{\partial E_g}{\partial P}\right|_{P=0} + \left.\frac{\partial E_{con}}{\partial P}\right|_{P=0} + \left.\frac{\partial E_{ex}}{\partial P}\right|_{P=0} \quad \text{(S4)}$$

a. Basic Model (based on literature values of PbS bulk modulus)

In the basic model, we take the first term in eqn.S4 to be pressure coefficient of the bulk energy gap, *i.e.:* -91.0 meV/GPa.[10]. The quantum confinement and Coulombic term of eqn. S4 reflect how pressure impacts the wave-function envelope and involve the change in NQD radius as in,

$$\left.\frac{\partial E_{con}}{\partial P}\right|_{P=0} = \frac{\hbar^2\pi^2}{2\mu}\left.\frac{\partial\left(\frac{1}{R^2}\right)}{\partial P}\right|_{P=0} = -\frac{\hbar^2\pi^2}{\mu R^2}\left.\frac{\partial R}{\partial P}\right|_{P=0} \quad \text{(S5)}$$

dR/dP can be related to the bulk modulus, B_0:

$$\frac{\partial R}{\partial P} = \frac{R_0^3}{3R^2}\frac{1}{V_0}\frac{\partial V}{\partial P} = -\frac{R_0^3}{3R^2}\frac{1}{B_0} \quad \text{(S6)}$$

R_0 and V_0 are the radius and volume of NQD under ambient pressure respectively. When $P \rightarrow 0$, $R = R_0$, then

$$\left.\frac{\partial R}{\partial P}\right|_{P=0} = -\frac{R_0}{3B_0} \quad \text{(S7)}$$

Substituting eqn. S7 into S5 yields

$$\left.\frac{\partial E_{con}}{\partial P}\right|_{P=0} = \frac{\hbar^2\pi^2}{3\mu B_0}\frac{1}{R_0^2} \quad \text{(S8)}$$

Similarly, the third term of the RHS of eqn. S4 can be written as:

$$\left.\frac{\partial E_{ex}}{\partial P}\right|_{p=0} = \left.\frac{\partial E_{ex}}{\partial R}\right|_{R=R_0}\left.\frac{\partial R}{\partial P}\right|_{p=0} = -\frac{1.8e^2}{\varepsilon_2 R_0^2}\frac{R_0}{3B_0} = --\frac{1.8e^2}{3\varepsilon_2 B_0}\frac{1}{R_0} \quad \text{(S9)}$$

Now we have the overall expression for $dE_{g,NQD}/dP$ by the basic model.

$$\left(\frac{\partial E_g^{NQD}}{\partial P}\right)_T = \left(\frac{\partial E_g}{\partial P}\right)_T + \frac{1}{3B_o}\left(\frac{\mathrm{h}^2\pi^2}{\mu R^2} - \frac{1.8e^2}{\varepsilon_2 R}\right) \tag{S10}$$

B_0 of bulk PbS was used in eqn. S10 (also eqn. 2). As shown in the blue dashed curve in Figure S5, the basic model overestimates the size-dependence of the pressure coefficient and does not provide a good fit to the experimentally observed trends.

b. Detailed Model (based on experimentally determined bulk moduli)

The detailed model accounts for the fact that the bulk modulus of PbS NQD differs from its bulk counterpart; this effect has important implications on the first term in eqn. S3 and S10 and is the main cause for the error of the basic model to account for the experimentally observed pressure dependence. Since the dependence of energy with lattice constant, *a*, is the same in a NQD as it is in the bulk, we can write:

$$\left(\frac{\partial E_g^{NQD}}{\partial a_{NQD}}\right)_T = \left(\frac{\partial E_g^{bulk}}{\partial a_{bulk}}\right)_T \tag{S11}$$

We can now express the impact of the size-dependent bulk modulus on the pressure coefficient in the form of the ratio:

$$\left(\frac{\partial E_g}{\partial P}\right)_T = \left(\frac{\partial E_g^{bulk}}{\partial P}\right)_T \frac{\left[\left(\frac{\partial P}{\partial a}\right)_T\right]_{bulk}}{\left[\left(\frac{\partial P}{\partial a}\right)_T\right]_{NQD}} = \left(\frac{\partial E_g^{bulk}}{\partial P}\right)_T \left(\frac{B_{o,bulk}}{B_{o,NQD}}\right)\left(\frac{a_{0,NQD}}{a_{0,bulk}}\right) \tag{S12}$$

$dE_{g,bulk}/dP = -91.0\ meV/GPa$ is known from literature[10]. Similar to the derivation of eqn. S7, da/dP can be derived from the definition of bulk modulus B_0:

$$\left.\frac{\partial a}{\partial P}\right|_{P=0} = -\frac{a_0}{3B_0} \tag{S13}$$

Then eqn. S12 is written as:

$$\left.\frac{\partial E_g}{\partial P}\right|_{P=0} = \left.\frac{\partial E_{g,bulk}}{\partial P}\right|_{P=0} \frac{B_{0,bulk}}{B_{0,NQD}} \frac{a_{0,NQD}}{a_{0,bulk}} \tag{S14}$$

Where $a_{0,bulk} = 5.929\ Å$ and $B_{0,bulk} = 52.9\ GPa$.[10] $a_{0,NQD}$ and $B_{0,NQD}$ were measured by WAXS (Table 1).

The second and third terms of eqn. S4 are the same as in the basic model except for substituting B_0 with $B_{0,NQD}$. Then we have the overall expression for $dE_{g,NQD}/dP$ by the detailed model:

$$\left.\frac{\partial E_{g,NQD}}{\partial P}\right|_{P=0} = \left.\frac{\partial E_{g,bulk}}{\partial P}\right|_{P=0} \frac{B_{0,bulk}}{B_{0,NQD}} \frac{a_{0,NQD}}{a_{0,bulk}} + \frac{\hbar^2\pi^2}{3\mu B_{0,NQD}} \frac{1}{R_0^2} - \frac{1.8e^2}{3\varepsilon_2 B_{0,NQD}} \frac{1}{R_0} \tag{S15}$$

Combining the quantities listed in Table 1, eqn. S15 was used to calculate $\left(\frac{\partial E_g}{\partial P}\right)_T$ of the three different PbS NQD sizes. Values of the three terms are given in Table 2. The calculated points were then fitted to spline for visual aid as presented by the red curve in Figure S5.

c. Basic Model with pressure-dependent effective mass.

In this section, we discuss the possible pressure dependence of effective mass and its influence on the pressure coefficient of energy gap. Assuming the reduced effective mass are also pressure-dependent and takes the form:[11]

$$\mu(P) = \mu(P=0)(1 + F_\mu^P \frac{1}{E_g(P=0)} \left(\frac{\partial E_g^b}{\partial P}\right)_T \hbar P) \tag{S16}$$

Where, E_g = *418 meV (293K)*[12] is the energy gap of bulk PbS, F is a dimensionless factor (fitted to be 0.35 for PbSe[11]). Then the confinement term in eqn. S4 now becomes:

$$\left.\frac{dE_{con}}{dP}\right|_{P=0} = \frac{\hbar^2\pi^2}{\mu(P=0)} \left(\frac{1}{3B_0} - \frac{F_\mu^P}{2E_g(P=0)} \left(\frac{\partial E_g^b}{\partial P}\right)_T\right) \frac{1}{R_0^2} \tag{S17}$$

Then the basic model was modified with the pressure dependent effective masses. Results by different F values are given in the following figures. Figure S6 shows the comparison of experimental data to the model for multiple values of F. The comparison of experiment and model illustrates that allowing for a pressure-dependent effective mass while maintaining the literature value of the bulk modulus does not yield a satisfactory fit. Below, we describe a model that accounts for both size-dependent bulk moduli and pressure-dependent effective mass.

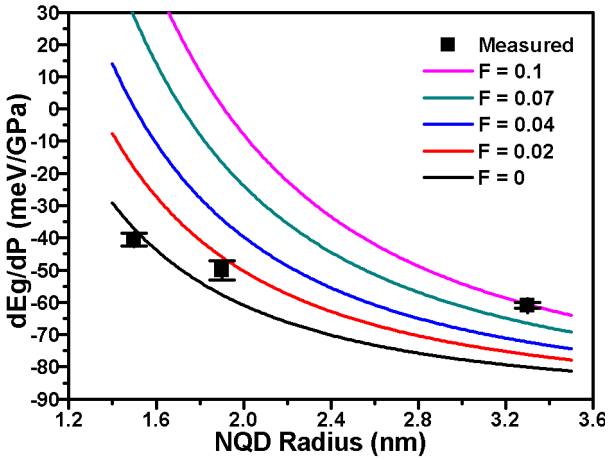

Figure S6. The size-dependent pressure variation of energy gap of PbS NQDs calculated by the basic model modified with pressure-dependent effective masses comparing with experimental values

d. Detailed Model With Pressure-Dependent Effective Mass.

Similar to the previous section, we here assume the reduced effective masses in the detailed model to be pressure dependent and take the form of eqn. S16. Figure S7 compares experimental values to the model for a range of values of *F*.

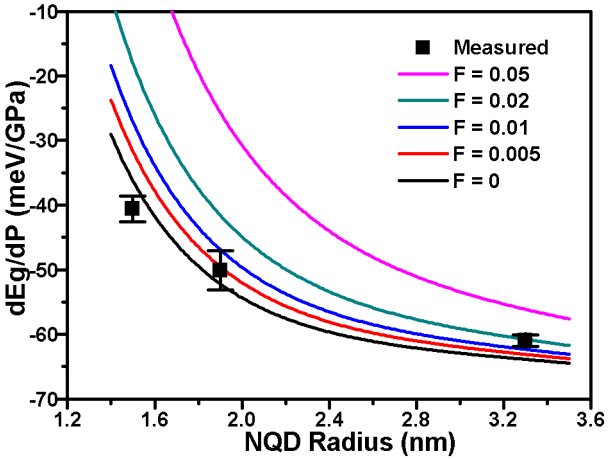

Figure S7. The size-dependent pressure variation of energy gap of PbS NQDs calculated by the modified detailed model with pressure-dependent effective masses comparing with experimental values

Figure S7 shows that the fitting was slightly improved by setting the pressure coefficient of effective mass *F* to a very small value (<0.01). This is expected due to the fact of introducing an additional tunable parameter. Also a small *F* indicates that the pressure dependence of the effective masses, if any, is insignificant and is not a denominating reason for the size dependent pressure coefficient of energy gap of NQDs.

8. WAXS spectra reveal the reversibility of the pressure-induced B1 to B16 structure transition.

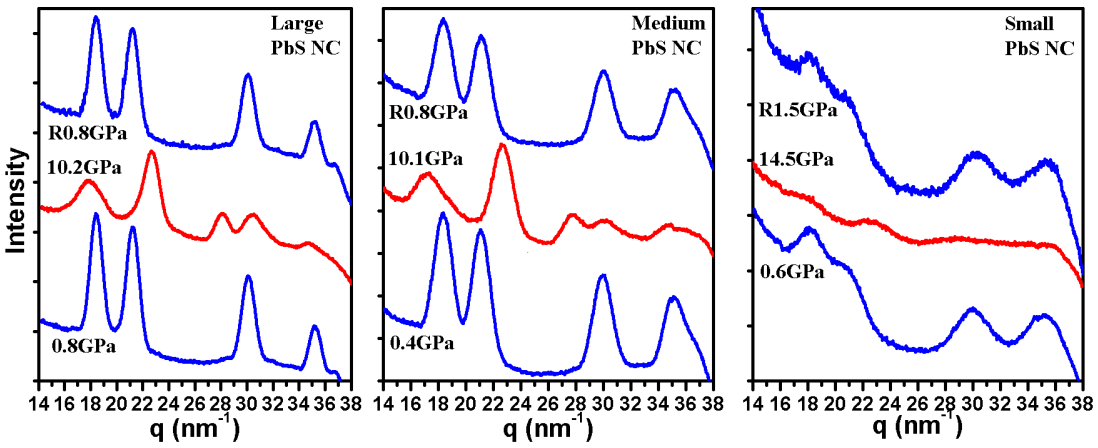

Figure S8. WAXS patterns of small, medium and large size NQD reveal the reversible, pressure-induced crystal structure transformation from rock-salt (low pressure, blue traces) to orthorhombic (high pressure, red traces).

9. References

(1) Hines, M. A.; Scholes, G. D. *Adv. Mater.* **2003**, *15*, 1844.

(2) Hammersley, A. P. *ESRF Internal Report, ESRF97HA02T* **1997**.

(3) Holland, T. J. B.; Redfern, S. A. T. *Mineralogical Magazine* **1997**, *61*, 65.

(4) Bian, K.; Wang, Z.; Hanrath, T. *Journal of the American Chemical Society* **2012**, *134*, 10787.

(5) Fei, Y.; Ricolleau, A.; Frank, M.; Mibe, K.; Shen, G.; Prakapenka, V. *Proceedings of the National Academy of Sciences* **2007**, *104*, 9182.

(6) Podsiadlo, P.; Lee, B.; Prakapenka, V. B.; Krylova, G. V.; Schaller, R. D.; Demortière, A.; Shevchenko, E. V. *Nano Letters* **2011**, *11*, 579.

(7) Lach-hab, M.; Papaconstantopoulos, D. A.; Mehl, M. J. *J. Phy. Chem. Solids* **2002**, *63*, 833.

(8) Brus, L. E. *The Journal of Chemical Physics* **1984**, *80*, 4403.

(9) Cuff, K. F.; Ellett, M. R.; Kuglin, C. D.; Williams, L. R. *Proceedings of the Seventh International Conference on the Physics of Semiconductors*; Dunod, Paris: Paris, 1964; Vol. 1.

(10) *LANDOLT-BORNSTEIN Numerical Data and Functional Relationships in Science and Technology New Series*; Madelung, O.; Schulz, M.; Weiss, H., Eds.; Springer: Berlin, 1983.

(11) Pedrueza, E.; Segura, A.; Abargues, R.; Bailach, J. B.; Chervin, J. C.; Martínez-Pastor, J. P. *Nanotechnology* **2013**, *24*, 205701.

(12) Preier, H. *Appl. Phys.* **1979**, *20*, 189.